BIOCHEMISTRY
including biophysical chemistry & molecular biology

Article

pubs.acs.org/biochemistry

Quantum Mechanics and Molecular Mechanics Study of the Catalytic Mechanism of Human AMSH-LP Domain Deubiquitinating Enzymes

Wenyou Zhu,[†] Yongjun Liu,[*,†] and Baoping Ling[‡]

[†]Key Laboratory of Colloid and Interface Chemistry, Ministry of Education, School of Chemistry and Chemical Engineering, Shandong University, Jinan, Shandong 250100, China

[‡]School of Chemistry and Chemical Engineering, Qufu Normal University, Qufu, Shandong 273165, China

Supporting Information

ABSTRACT: Deubiquitinating enzymes (DUBs) catalyze the cleavage of the isopeptide bond in polyubiquitin chains to control and regulate the deubiquitination process in all known eukaryotic cells. The human AMSH-LP DUB domain specifically cleaves the isopeptide bonds in the Lys63-linked polyubiquitin chains. In this article, the catalytic mechanism of AMSH-LP has been studied using a combined quantum mechanics and molecular mechanics method. Two possible hydrolysis processes (Path 1 and Path 2) have been considered. Our calculation results reveal that the activation of Zn^{2+}-coordinated water molecule is the essential step for the hydrolysis of isopeptide bond. In Path 1, the generated hydroxyl first attacks the carbonyl group of Gly76, and then the amino group of Lys63 is protonated, which is calculated to be the rate limiting step with an energy barrier of 13.1 kcal/mol. The energy barrier of the rate limiting step and the structures of intermediate and product are in agreement with the experimental results. In Path 2, the protonation of amino group of Lys63 is prior to the nucleophilic attack of activated hydroxyl. The two proton transfer processes in Path 2 correspond to comparable overall barriers (33.4 and 36.1 kcal/mol), which are very high for an enzymatic reaction. Thus, Path 2 can be ruled out. During the reaction, Glu292 acts as a proton transfer mediator, and Ser357 mainly plays a role in stabilizing the negative charge of Gly76. Besides acting as a Lewis acid, Zn^{2+} also influences the reaction by coordinating to the reaction substrates (W1 and Gly76).

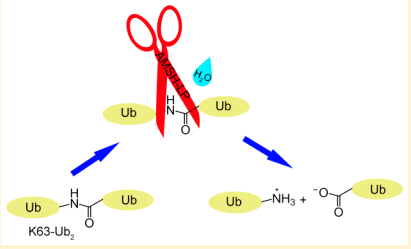

Ubiquitin (Ub) is a small protein that exists in all tissues of eukaryotic organisms.[1−5] It performs its myriad functions by ubiquitination, which is an enzymatic and post-translation modification process involving three sequential steps: activation, conjugation, and ligation, performed by ubiquitin-activating enzymes (E1s), ubiquitin-conjugating enzymes (E2s), and ubiquitin ligases (E3s),[6−8] respectively. Through the above sequential reactions, the ubiquitin molecule is ligated with the lysine residues of the substrate protein by an isopeptide bond or with the amino group of the N-terminus of protein by a peptide bond.[9] These protein modifications may occur in either a single ubiquitin protein (monoubiquitination) or a chain of ubiquitin (polyubiquitination), by which the ubiquitin molecules are attached to the lysine residues in ubiquitin itself.[10] As the ubiquitin molecule contains seven lysine residues, each of them can bind with the terminal carboxyl group of another ubiquitin whereby at least seven distinct ubiquitin chain linkage types (lysine-6, -11, -27, -29, -33, -48, and -63) can be formed in polyubiquitination, increasing the complexity of ubiquitination.[11−15] Among them, the Lys48-linked ubiquitin chains are the most abundant linkages *in vivo* and constitute the canonical signal for proteasomal degradation.[4,10] The roles of ubiquitin chains linked by residues other than Lys 48 are still not fully understood yet. But the Lys 63-linked ubiquitin chains play proteasome-independent roles in a variety of intracellular events, such as DNA repair, inflammatory signaling, and ribosomal protein synthesis.[3,10,16,17]

Similar to other post-translational modification, ubiquitylation is also a reversible process that can be controlled and regulated through the deubiquitination process catalyzed by deubiquitinating enzymes (DUBs: also named deubiquitinases).[18−20] DUBs belong to the isopeptidases family, which catalyzes the hydrolysis of peptide (isopeptide) bond between ubiquitin molecules, as shown in Scheme 1, and removes the covalently linked ubiquitin molecules from the target substrates. On the basis of previous studies, about 90 DUBs can be encoded by the human genome, and approximately 80 DUBs are predicted to be active.[10] According to the different functions and sequences, the DUBs family can be classified

Scheme 1. Hydrolysis Process of Isopeptide Bond Catalyzed by DUBs

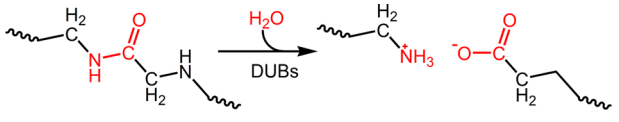

Received: May 14, 2015
Revised: July 16, 2015
Published: August 10, 2015

DOI: 10.1021/acs.biochem.5b00527
Biochemistry 2015, 54, 5225−5234

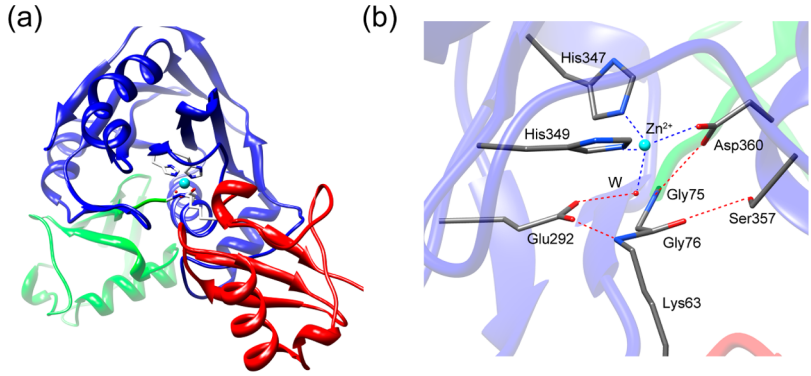

Figure 1. (a) The superposed structure of AMSH-LP-Zn^{2+} and AMSH-LP-K63Ub_2 complexes; (b) Tthe active site structure of AMSH-LP.

into five groups: ubiquitin carboxy-terminal hydrolases (UCHs), ubiquitin-specific proteases (USPs), Otubain proteases (OTUs), Machado−Joseph disease proteases (MJDs), and JAB1/MPN/Mov34 metalloenzymes (JAMMs).[21,22] All DUBs except JAMMs are cysteine proteases, whereas JAMMs are zinc metalloproteases which require a Zn^{2+} for catalysis.[21,23]

AMSH (associated molecule with the SH3 domain of signal transducing adaptor molecule (STAM)) family members are JAMMs DUBs, which specifically cleave the isopeptide bonds of Lys63-linked polyubiquitin chains from the conjugated substrates to regulate various cellular processes.[6,24,25] It has been proposed that AMSH enzymes facilitate the recycling of receptors and act as key regulators of the endosomal sorting complexes required for transport (ESCRTs).[25,26] Although many structures of DUBs have been reported, the mechanism of linkage-specific polyubiquitin cleavage for all DUBs is still unclear owing to the lack of structures of DUBs in complex with the isopeptide-linked ubiquitin chains.[11,12,27−30] In 2008, the human AMSH-LP DUB in complex with Lys63-linked diubiquitin (K63−Ub_2) (PDB code: 2ZNV) and with Zn^{2+} (PDB code: 2ZNR) have been successfully crystallized at 1.6 and 1.2 Å resolutions,[31] respectively. In the crystal structure of AMSH-LP DUB-Zn^{2+} complex, Zn^{2+} is stabilized in the active site by forming coordinate bonds with residues His347, His349, Asp360 and a water molecule which is hydrogen bonded to Glu292. In the crystal structure of AMSH-LP DUB-K63-Ub_2 complex, the isopeptide bond between the amino group of Lys63 in the proximal ubiquitin and the carbonyl group of Gly76 in the distal ubiquitin is stabilized in the active pocket by a complex hydrogen bonding network. It should be noted that, in order to obtain the crystal structure of AMSH-LP DUB-K63-Ub_2 complex, the residue Glu292 had been mutated to Ala292 to make the protein inactive. These two crystal structures provide the structural basis for understanding the selective cleavage of Lys63-linked ubiquitin chains by AMSH-LP family members; however, the reaction details of AMSH-LP are still unknown.[6,31] Thus, in this article, on the basis of the obtained structures, a reactant model was constituted, and the reaction detail was investigated by using the quantum mechanical/molecular mechanical (QM/MM) method.[32,33]

The hydrolysis processes of peptides (isopeptides) bond catalyzed by some other zinc-containing enzymes have been studied by using the QM/MM calculations, and different mechanisms have been proposed. For example, in the QM/MM studies of carboxypeptidase A (CPA)[34] and angiotensin-converting enzyme (ACE),[35] Xu and co-workers proposed that the activation of Zn^{2+}-bound water molecule and the nucleophilic attack by the hydrolytic water proceed in a concerted manner, whereas in the studies of insulin degrading enzyme (IDE),[36] Prabhakar and co-workers suggested that these two steps proceed in a stepwise manner. For the hydrolysis process of isopeptide bond catalyzed by AMSH-LP, it is still unclear how the catalytic reaction occurs. In addition, several questions for the catalytic reaction details have no answers yet. For instance, which reaction step is rate limiting and how Zn^{2+} influences the reaction are still unknown. Theoretical study on the mechanism of AMSH-LP can deepen our understanding of the catalytic properties of AMSH-LP and other JAMMs DUBs enzymes. To our knowledge, this is the first theoretical report of the catalytic mechanism of AMSH-LP.

METHODS

Computational Models. The computational model was constructed on the basis of crystal structures of AMSH-LP in complex with K63-Ub_2 (PDB code: 2ZNV) and Zn^{2+} (PDB code: 2ZNR).[31] To construct the reaction center, the structures of AMSH-LP in complex with K63-Ub_2 and Zn^{2+} were first superposed by the UCSF Chimera package.[37] The small root-mean-square deviation (RMSD) valve (0.472 Å) of the superposition indicates that the active site architectures of the two crystal structures are basically identical, as shown in Figure 1a. According to the superposition, the reaction center was constructed, which includes Zn^{2+}, K63-Ub_2, residue Glu292, and a Zn^{2+}-coordination water molecule, as shown in Figure 1b. One can see that Zn^{2+} directly coordinates to His347, His349, Asp360, and the water molecule (W). Glu292 interacts indirectly with Zn^{2+} by a water mediator. A hydrogen bonding network is formed between K63-Ub_2 and residues Gly75, Glu292, and Ser357. The protonation states of titratable residues were assigned by using PROPKA3.1 package[38−41] under the experimental conditions. According to the predicated pK_a values, His347, His349, and other histidine residues were set to their deprotonation states, whereas the other residues were set to their normal protonation states. The HBUILD program was used to add the missing hydrogen atoms in CHARMM package.[42] Afterward, the model was placed into the TIP3P[43] water, which forms a water sphere with the radius of 42 Å. When the system is solvated, the origin of the system is fixed on the center of the longest axis of protein. After neutralized by one sodium ion and a sequence of minimization steps, a 20 ns MD simulation was performed with the CHARMM22/CMAP all-atom force field.[42,44,45] The prepared system was divided into two regions: an outer buffer region (36 Å < r < 42 Å) and an inner reaction region (r < 36 Å), which

DOI: 10.1021/acs.biochem.5b00527
Biochemistry 2015, 54, 5225−5234

were characterized by Langevin dynamics with friction and random force and Newton's equations of motion, respectively. During the MD simulation, the stochastic boundary condition[46] at 1 atm and 298.15 K was used as a thermal bath to keep the stability of system and to avoid the escape of water molecules from dynamic region. The 20 ns MD simulation was carried out by three steps: first, the prepared system was heated for 50 ps from 0 to 298.15 K with a time step of 1 fs; then, the system was equilibrated for 50 ps with the same time step at 298.15 K; finally, a 20 ns MD simulation was performed.

QM/MM Calculations. Two typical snapshots taken from a 20 ns MD simulation were used for the subsequent QM/MM calculations. During the QM/MM calculations, the whole systems were divided into two regions: QM and MM. QM region contains 86 atoms, including the side chains of Glu292, His347, His349, Asp360, and Ser357 of AMSH-LP, Lys63 in the proximal ubiquitin, Gly76 and Gly75 in the distal ubiquitin, part of the residue Arg74 in distal ubiquitin, a water molecule and Zn^{2+}. The rest of the atoms of the system were put into the MM region. The interfaces between the two subsystems were treated by hydrogen linked atoms with the charge shift model.[47] For a better description of hydrogen bonding interaction between the small $-CH_2OH$ group of Ser357 and the carbonyl oxygen of Gly76, one backbone carbon atom was also included in the QM region, and therefore two link H atoms were inserted. Although the current link-atom approach cannot account well for the backbone atoms, the $-CH_2OH$ group is not directly involved in the chemical reaction, and the inserted link atoms are far from the reaction center, we assume that the caused error would be very small. An electronic embedding scheme[48] where the MM subsystem charges were combined into the one-electron Hamiltonian of QM calculations was implemented to characterize the polarizing effects of environments on the QM region. The QM subsystem was performed in Turbomole[49] with DFT at B3LYP functional.[50,51] The MM subsystem was treated by using CHARMM22 force field[45] in DL-POLY.[52] ChemShell package[53] was used to combine the Turbomole and DL-POLY programs. All the geometries were optimized by HDLC optimizer.[54] The L-BFGS method[55,56] was applied to find the local minima. Transition states were searched by the P-RFO algorithm[57] with the following eigenmodes of the Hessian. All transition states were determined by only one negative eigenvalue. Except Zn^{2+}, all geometry optimizations of the QM subsystem were treated at the 6-31G(d,p) level. For Zn^{2+}, the Stuttgart ECP/basis set (SDD)[58] was used to describe the Zn^{2+} coordination shell. Single point energies were performed at the higher level (SDD, 6-31++G(d,p)) on the basis of the optimized structures. To obtain more accurate energies, the DFT-D3 program[59] was applied to describe the dispersion interaction. During the calculations, the residues of MM region within 17.0 Å of carbonyl carbon atom of Gly76 in the distal ubiquitin were allowed to move, while the rest of the residues were frozen.

RESULTS AND DISCUSSION

Structures of AMSH-LP. The constructed computational model was first performed a 20 ns MD simulation. The RMSD of AMSH-LP derived from the 20 ns MD simulation is displayed in Figure 2. One can see that the system is basically equilibrated after 12 ns, which implies that a 20 ns MD simulation is adequate for equilibrating the system. The equilibrated RMSD of AMSH-LP is maintained about at 1.16 Å. After the system achieves the equilibration, two typical

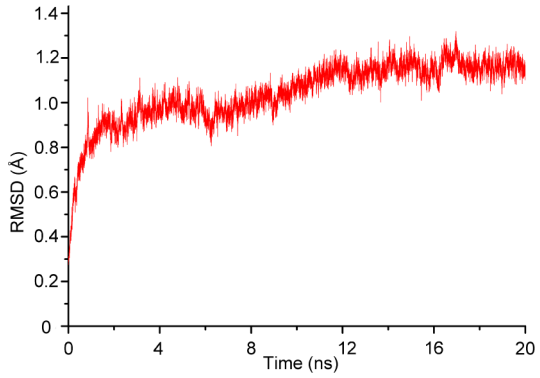

Figure 2. Time dependence of RMSD from 20 ns MD simulations.

structures can be obtained, as shown in Figure 3, in which Zn^{2+} directly ligates to residues His347, His349, Asp360, and a water

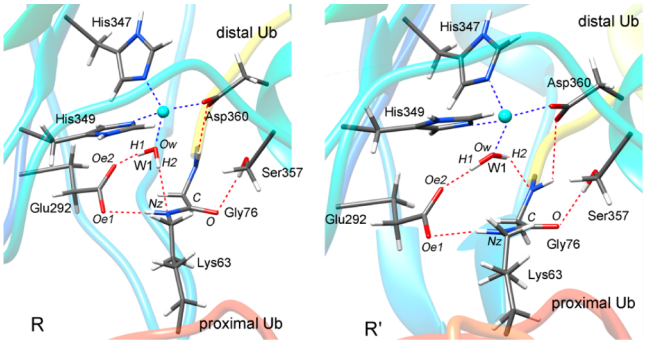

Figure 3. Two typical structures of active sites (R and R′).

molecule (W1). Glu292 forms one hydrogen bond with W1. The amino group of Lys63 in proximal ubiquitin is hydrogen bonded to Glu292. Two hydrogen bonds are formed between Gly76 in distal ubiquitin and Asp360 and Ser357. In the structure of R, W1 also forms one hydrogen bond with the amino group of Lys63. But in the structure of R′, W1 forms one hydrogen bond with the amino group of Gly76. The main difference between R and R′ is the orientation of W1. On the basis of the time course of the distance of H···Nz between the hydrogen atom of W1 and Nz atom of Lys63 (Figure S1), the percentage of the structures like R is estimated to be approximately 60% of the equilibrated structures.

Using R as the initial reactant, the reaction details of AMSH-LP were calculated by using the QM/MM method. It should be noted that several experimental studies have been conducted to explore the hydrolysis processes of isopeptide bond by AMSH-LP. For example, the mutation experiments have revealed that the Glu292Ala mutant is completely inactive.[31] Besides, in the studies of thermolysin[60] and AMSH,[6] which are similar to AMSH-LP, the corresponding intermediate analogue and product have been crystallized. According to the previous studies,[6,31] two possible hydrolysis processes of isopeptide bond were considered (Scheme 2). As shown in Scheme 2, the water molecule which coordinates to Zn^{2+} is first activated by residue Glu292. Then, the activated hydroxyl directly attacks the carbonyl group of Gly76, leading to the cleavage of the isopeptide bond, which is illuminated in Path 1. Alternatively, the amino group of Lys63 is first protonated by Glu292, and then the C−Nz bond is cleaved, as shown in Path 2.

DOI: 10.1021/acs.biochem.5b00527
Biochemistry 2015, 54, 5225−5234

Scheme 2. Proposed Mechanisms for AMSH-LP

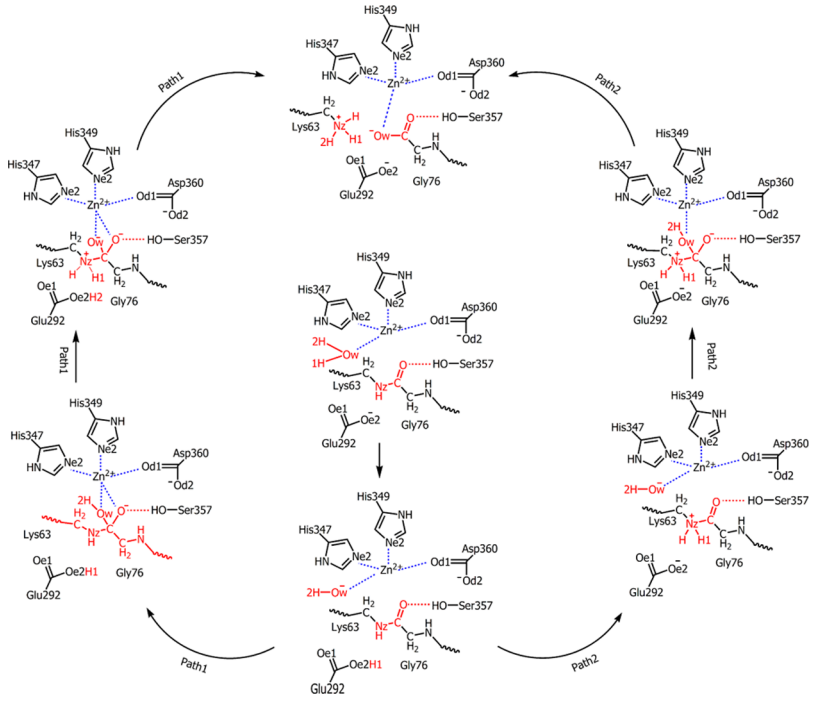

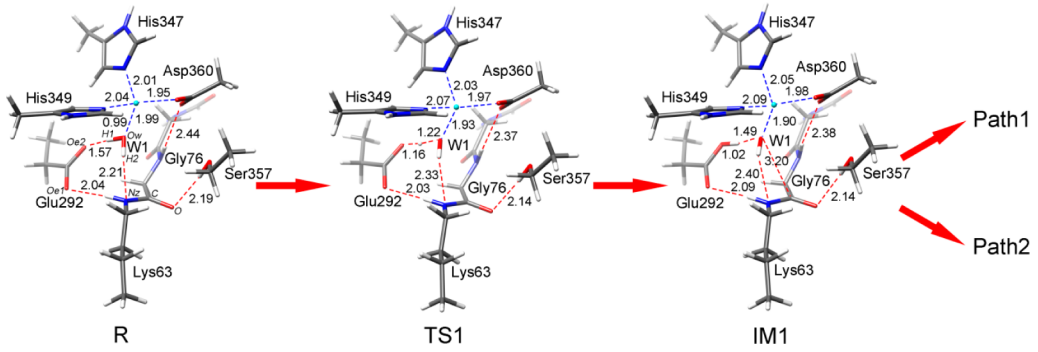

Figure 4. Optimized structures of reactant, transition state, and intermediate in the activation process of W1. The distances are given in angstroms.

Calculated Reaction Mechanism of AMSH-LP. The structure of R was first used as the reactant. The catalytic reaction is initiated by the activation of the water molecule (W1). The optimized structures of reactant, transition state, and intermediate for the activation process are shown in Figure 4, and the energy profile is displayed in Figure 5. As shown in R, a strong hydrogen bond is formed between W1 and Glu292 with length of H1−Oe2 of 1.57 Å, facilitating the activation of W1. In TS1, the distance between H1 and Oe2 further decreases to 1.16 Å. In IM1, the H1 atom of W1 is completely transferred to the carboxyl group of Glu292, and the water molecule (W1) has been activated into a hydroxyl ion. Along with the proton transfer, the coordination bonds between Zn^{2+} and residues are well kept. The activation of W1 is calculated to be quite easy with an energy barrier of only 3.9 kcal/mol. Following the activation of W1, two hydrolysis processes of the isopeptide bond are explored in the next section.

Path 1. The optimized structures of intermediates, transition states, and product in Path 1 are shown in Figure 6. The generated hydroxyl first attacks the carbonyl group of Gly76 in the distal ubiquitin. In TS2-1, the distance between Ow atom of hydroxyl and C atom of Gly76 decreases to 1.88 Å from 3.20 Å

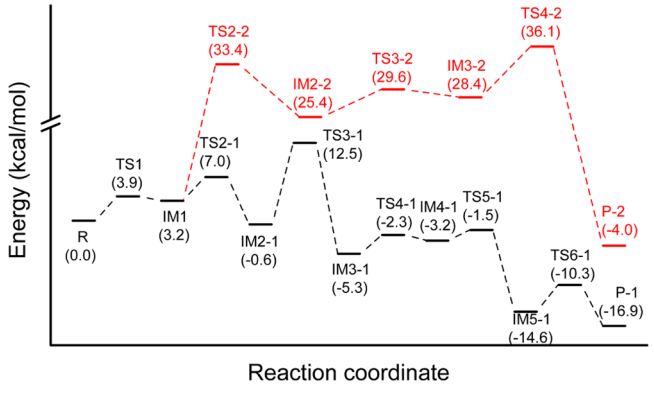

Figure 5. Energy profiles of the catalytic reaction. The energy data have included the dispersion corrections.

in IM1. In IM2-1, the hydroxyl group has been attached to the carbonyl C atom, forming a tetrahedral intermediate, in which the distance of Ow−C changes to 1.44 Å. We also note that the ligand environment of Zn^{2+} has been changed from TS2-1 to IM2-1. In TS2-1, a transitory pentacoordinate of Zn^{2+} is formed. But in IM2-1, the newly formed oxyanion of Gly76

DOI: 10.1021/acs.biochem.5b00527
Biochemistry 2015, 54, 5225−5234

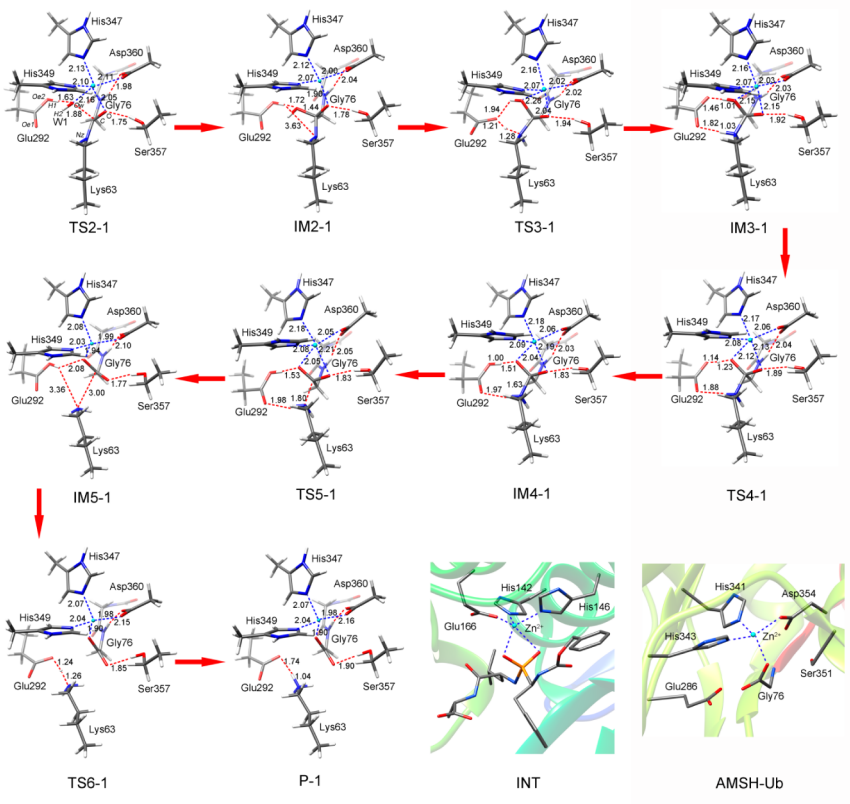

Figure 6. Optimized structures of the intermediates, transition states, and product in Path 1. The distances are given in angstroms. INT represents a crystallized intermediate analogue of thermolysin (PDB code: 4TMN).

replaces the hydroxyl to coordinate with Zn^{2+}. In addition, the hydrogen bond distance between Ser357 and Gly76 decreases from 2.14 Å in IM1 to 1.78 Å in IM2-1, suggesting this hydrogen bond becoming stronger. In other words, Ser357 may play an important role in stabilizing the negative charge of Gly76. The energy barrier of the formation of the Ow−C bond is 3.8 kcal/mol, which means that the formation of IM2-1 is also quite easy.

As described above, the activation of W1 and the nucleophilic attack by generated hydroxyl may also occur in a concerted manner. To confirm whether the activation of W1 is concerted with the formation of the Ow−C bond, the potential energy surface (PES) including the abstraction of H1 by Glu292 and the formation of Ow-C bond has been calculated, which is shown in Figure 7. In Figure 7, the horizontal axis and vertical axis respectively represent the cleavage of the Ow−H1 bond and formation of the Ow−C bond. The reaction coordinate of the Ow−H1 bond changes from 0.97 to 1.72 Å with an increment of 0.05 Å, and that of the Ow−C bond varies from 1.44 to 3.09 Å with the same increment. Three low-energy regions and two saddle points can be recognized in Figure 7. The structures located at the upper left, upper right, and lower right corners represent the structures of R, IM1, and IM2-1, respectively. It can be seen that W1 is first activated, and then the nucleophilic attack of hydroxyl occurs. The activation of W1 is an essential step for the catalytic reaction of AMSH-LP.

After the formation of IM2-1, the amino group of Lys63 in the proximal ubiquitin is protonated by the nearby residue Glu292 to generate IM3-1, which corresponds to an energy barrier of 13.1 kcal/mol, as shown in Figure 5. From IM2-1 to IM3-1, the distance between H1 of carboxyl group of Glu292 and Nz atom of Lys63 decreases from 3.63 to 1.03 Å via 1.28 Å

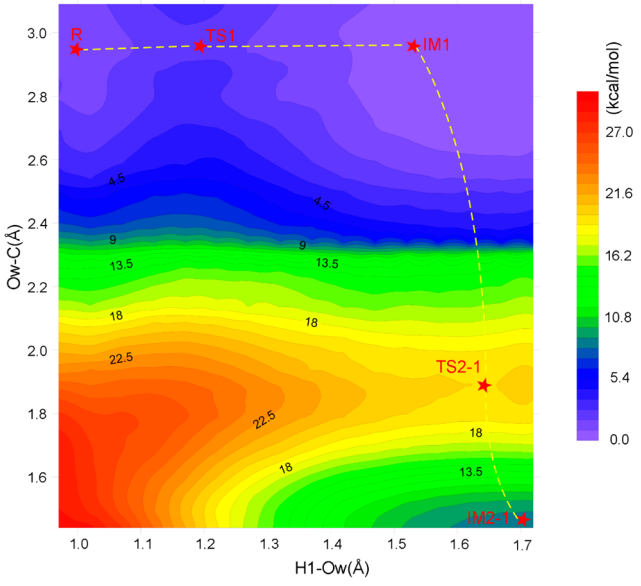

Figure 7. PES calculated at the B3LYP/6-31G(d,p) level using distances H1−Ow and Ow−C as reaction coordinates.

in TS3-1. Accompanying this proton transfer, a hydrogen bond is formed between the carboxyl oxygen of Glu292 and the amino group of substrate. Meanwhile, two oxygen atoms of Gly76 coordinate to Zn^{2+}, forming a stable pentacoordinate in TS3-1 and IM3-1. The pentacoordinate around Zn^{2+} was also found in the reaction intermediate analogue of thermolysin (PDB code: 4TMN).[60] Thermolysin is also a Zn^{2+}-containing metalloprotease, which has a active site similar to AMSH-LP. In

DOI: 10.1021/acs.biochem.5b00527
Biochemistry 2015, 54, 5225−5234

the intermediate analogue of thermolysin, Zn^{2+} coordinates to residues His142, His146, Glu166, and the two oxygen atoms of substrate, forming pentacoordinate as shown in Figure 6 (INT). This implies that the optimized pentacoordinate is not unprecedented in Zn^{2+}-containing metalloproteases. The hydrogen bonds and ligand environments around the active site make the intermediate (IM3-1) more stable than IM2-1.

In the next step, Glu292 acts as the proton acceptor again. The hydroxyl proton of Gly76 transfers to the carboxyl group of Glu292, forming intermediate IM4-1. This transfer process corresponds to a low energy barrier of 3.0 kcal/mol. Although IM4-1 is structurally similar to IM3-1, the relative energy of IM4-1 is higher than that of IM3-1 by 2.1 kcal/mol, which is probably due to the repulsion of the two oxyanions attached to the same sp3 hybridized carbon. As a result, the following cleavage of isopeptide bond is very easy. As shown in Figure 5, the cleavage of the C−Nz bond corresponds to an energy barrier of 1.7 kcal/mol. In IM5-1, the distance of the C−Nz bond increases to 3.00 Å from 1.63 Å in IM4-1 via 1.80 Å in TS5-1. With the cleavage of the isopeptide bond, Zn^{2+} returns to tetracoordinate again. Up to now, the diubiquitin chain is cleaved to two free ubiquitin chains, making the system (IM5-1) more stable. To better understand the cleavage of the isopeptide bond, the PES as a function of reaction coordinate of C−Nz bond and H2−Oe2 bond was further calculated. As shown in Figure 8, the horizontal axis describes the proton

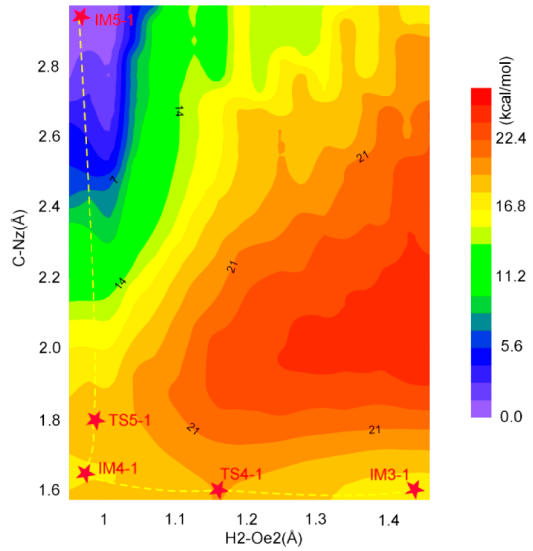

Figure 8. PES calculated at the B3LYP/6-31G(d,p) level using distances H2−Oe2 and Nz−C as reaction coordinates.

transfer from Gly76 to Glu292, and the vertical axis represents the cleavage of the C−Nz bond. The distance of the C−Nz bond changes from 1.57 to 2.97 Å with an increment of 0.05 Å, and the length of H2−Oe2 changes from 0.95 to 1.46 Å with an increment of 0.03 Å. Three low energy regions located at the lower-right, lower-left, and upper-left corners represent IM3-1, IM4-1, and IM5-1, respectively. One can see that the proton on the hydroxyl group of Gly76 first transfers to the carboxyl group of Glu292, and then the C−Nz bond cleaves. The proton transfer is the prerequisite for the cleavage of the C−Nz bond.

In the last step of Path 1, the amino group of Lys63 is protonated by Glu292 to generate P-1, which corresponds to an energy barrier of 4.3 kcal/mol. In P-1, the carboxyl oxygen atom of Gly76 replaces W1 to coordinate with Zn^{2+}, forming a tetracoordinate state. The obtained structure of P-1 is in good agreement with the crystal structure of AMSH in complex with the product (AMSH-Ub).[6] AMSH also belongs to the JAMMs DUBs enzymes and has a structure similar to AMSH-LP. In the crystal structure of AMSH-Ub, the carboxyl group of Gly76 replaces the Zn^{2+}-bound water molecule to coordinate with Zn^{2+} to maintain its tetrahedral coordination.

In addition, the structures and energies of MM region may be changed differently along with the progress of the chemical reaction, which can be easily monitored by comparing the MM energies of the involved species. The energies of the MM region along the Path 1 (Figure 6) have been displayed in Figure S2. One can see that the relative MM energies show different characteristics. From TS2-1 → TS3-1, the MM energies only change slightly. However, from IM2-1/TS3-1 to IM3-1 and from IM5-1 to TS6-1/P-1, the MM energies show clear changes of about 5−7 kcal/mol. In both of the above processes, the proton transfers are involved between Glu292 and the amino group of Lys63 in the proximal ubiquitin, which cause large conformational changes of the carboxyl group of Glu292; accordingly, the MM structures and energies of the involved species show large fluctuation.

Path 2. An alternative pathway (Path 2), as described in Scheme 2, was also explored, in which the protonation of amino group of Lys63 by Glu292 is prior to the cleavage of the C−Nz bond. The optimized structures of intermediates, transition states, and product are shown in Figure 9. One can see that, after the activation of W1, the carboxyl proton of Glu292 first transfers to the amino group of Lys63, generating IM2-2 via TS2-2. We also note some structural changes during the proton transfer. In particular, from IM1 to IM2-2, the distance between the Ow of activated hydroxyl and the carbonyl C atom of Gly76 decreases from 3.20 to 2.57 Å, and the hydrogen bond formed by Glu292 and the activated hydroxyl no longer exists, which is replaced by a new one between Ser357 and the activated hydroxyl. The protonation of amino group of Lys63 by Glu292 is calculated to be difficult with an energy barrier of 30.2 kcal/mol (Figure 5).

Following the protonation of Lys63, the activated hydroxyl attacks on the carbonyl group of Gly76, and simultaneously the C−Nz bond of the diubiquitin chains cleaves, generating intermediate IM3-2. From Figure 9, one can see that the formation of the Ow−C bond and cleavage of the C−Nz bond proceed in a concerted but asynchronous manner. As shown in the transition state TS3-2, the formation of the Ow−C bond is prior to the cleavage of the C−Nz bond. In TS3-2, the Ow−C bond is basically formed with a distance of 1.41 Å, but the cleavage of the C−Nz bond is still in progress. The energy barrier of this step is calculated to be 4.2 kcal/mol (Figure 5). It should be noted that the pentacoordination of Zn^{2+} found in Path 1 no longer exists. In the last step, the proton of Gly76 transfers to the amino group of Lys63 with an energy barrier of 7.7 kcal/mol. In P2-2, Lys63 forms two hydrogen bonds with Glu292 and Gly76. So far, the hydrolysis process of the isopeptide bond has been completed.

In summary, Path 1 is the most possible reaction pathway, in which the protonation of Lys63 by Glu292 is calculated to be rate limiting with an energy barrier of 13.1 kcal/mol. According to the measured k_{cat} (0.86 ± 0.07 s^{-1}) of AMSH-LP, the estimated free energy barrier is 17.6 kcal/mol. Considering the B3LYP method normally underestimates the barrier heights by a few kilocalories per mole, the calculated energy barrier of Path 1 is basically in agreement with the experimental result. In

DOI: 10.1021/acs.biochem.5b00527
Biochemistry 2015, 54, 5225−5234

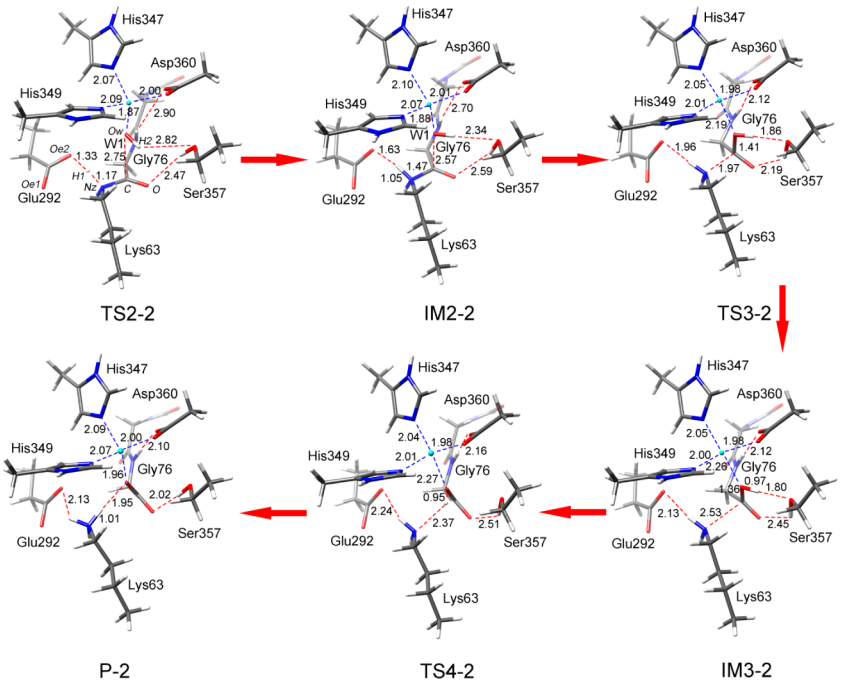

Figure 9. Optimized structures of the intermediates, transition states, and product in Path 2. The distances are given in angstroms.

addition, the obtained structures of intermediates and product in Path 1 are very similar to the crystal structures of similar enzymes. In Path 2, the two proton transfer processes correspond to the higher barriers (33.4 and 36.1 kcal/mol), and therefore Path 2 can be ruled out.

As described above, two typical equilibrated structures, namely, R and R′, are found from the MD simulation. However, the main difference between R and R′ is the orientation of W1, which may cause some difference in the activation of hydrolytic water molecule. After the activation of water molecule, the subsequent reaction steps would be very similar; therefore, for the structure of R′, only the activation process was studied. The optimized structures of the activation process are shown in Figure S3 of Supporting Information, and the energy profile is shown in Figure S4. The energy barrier for the activation of water is calculated to be 6.0 kcal/mol, which is higher than that in Path 1 by 2.1 kcal/mol. Since the structure of IM1′ is very similar to that of IM1, the following elementary steps are supposed to be much alike.

Influence of Zn^{2+} and the Electrostatic Effect of Environment. Zn^{2+} plays an important role in the catalytic reaction. It is necessary to analyze the changes of charges of Zn^{2+} and Zn^{2+}-coordinated residues. The ESP charges of key QM atoms in Path 1 were calculated by using QM/MM method, which are shown in Figure 10 and Table S1. The calculation results reveal that Zn^{2+} always distributes its positive charge to the ligand molecules. In particular, before the formation of IM3-1, the charge of Zn^{2+} displays a considerable variation. It is probably due to the changes of Zn^{2+}-coordinated structures. As shown in Figures 4 and 6, from R to IM2-1, the ligand water (W1) is activated into a hydroxyl group, which is then replaced by an oxygen ion to form a transitory pentacoordinate state (TS2-1). From IM2-1 to IM3-1, the protonated amino group further replaces the oxygen ion and competes with Zn^{2+} to delocalize the negative charge of the substrate, increasing the positive charge of Zn^{2+}. On the whole, the charge of Zn^{2+} changes between 0.51 au and 1.16 au (Table S1), indicating that Zn^{2+} acts as a Lewis acid to participate in the reaction. As for the charges of other residues, two Ne2 atoms of His347 and His349 display some changes during the catalytic reaction, but the Od1 atom of Asp360 is basically undisturbed.

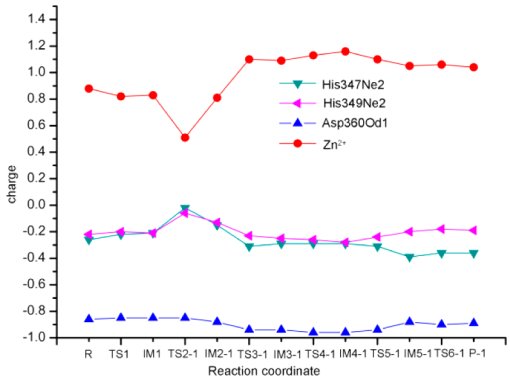

Figure 10. ESP charges of Zn^{2+} and its ligated atoms of residues.

Besides, the changes of distances between Zn^{2+} and its ligated atoms are also examined, which are shown in Figure 11. One can see that the distances between Zn^{2+} and the oxygen atoms of Gly76 and W1 change significantly, which reflects that the coordination structure undergoes reorganization during the catalytic cycle. At the beginning of the reaction, Gly76 does not coordinate with Zn^{2+}. However, with the formation of the transitory pentacoordinate structure (TS2-1), the distance between Zn^{2+} and the O atom of Gly76 decreases from ∼5.0 Å to ∼2.0 Å, and the distance between Zn^{2+} and the Ow atom of hydroxyl increases from 1.90 Å in IM1 to 2.75 Å in IM2-1 (the data is not shown in Figure 6). The other three residues always coordinate with Zn^{2+}. In general, the ligated environment around Zn^{2+} in these intermediates and transition states changes between pentacoordinate and tetracoordinate states, suggesting that, besides acting as a Lewis acid, Zn^{2+} also influences the reaction by coordinating to the reaction

DOI: 10.1021/acs.biochem.5b00527
Biochemistry 2015, 54, 5225−5234

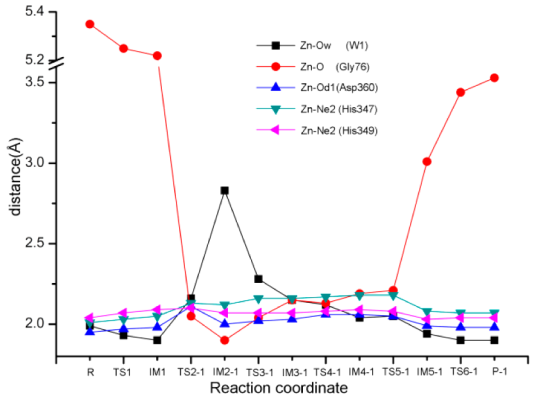

Figure 11. Distances between Zn^{2+} and its ligated atoms.

substrates (W1 and Gly76). The pentacoordinate state plays an important role in the stabilization of intermediates and transition states.

CONCLUSIONS

In this work, the cleavage mechanism of the isopeptide bond catalyzed by AMSH-LP has been studied by using the QM/MM method. According to the different orientations of hydrolytic water (W1) in the active site, two computational models (R and R′) were constructed. It was found that the different orientations of W1 in model R and R′ only slightly influence the activation of hydrolytic water. On the basis of the structure of R, two possible hydrolytic pathways (Path 1 and Path 2) of the isopeptide bond were considered. Path1 includes six elementary steps. The crystal water (W1) is first activated by Glu292, and then the generated hydroxyl attacks the carbonyl group of Gly76 in the distal ubiquitin. The following protonation of the amino group of Lys63 is the prerequisite for the cleavage of the isopeptide bond. This protonation process is calculated to be rate limiting for the overall catalytic reaction, with an energy barrier of 13.1 kcal/mol, which is close to the estimated free energy barrier of 17.6 kcal/mol from the experiment. In Path 2, the protonation of amino group of Lys63 is assumed to be prior to the nucleophilic attack of activated hydroxyl, but the calculated barrier of this protonation is as high as 33.4 kcal/mol, and therefore Path 2 can be ruled out.

According to our calculations, Zn^{2+} plays an important role in the catalytic reaction. Besides acting as Lewis acid, Zn^{2+} also influences the reaction by regulating its ligated environment. During the catalytic reaction, Glu292 acts as the proton donor/acceptor, and Ser357 has the function to stabilize the negative charge in Gly76. These results may provide useful information for the regulation of enzyme activity.

ASSOCIATED CONTENT

Supporting Information

The Supporting Information is available free of charge on the ACS Publications website at DOI: 10.1021/acs.biochem.5b00527.

ESP charges of Zn^{2+} and its ligated atoms of residues, the time course of the distance between the hydrogen atom of W1 and Nz atom of Lys63 taken from the MD simulation, the relative energies of the MM region along with Path 1, and the optimized structures and energy profile of activation of Zn^{2+}-bound water molecule by using R′ as the reactant (PDF)

AUTHOR INFORMATION

Corresponding Author

*Tel.: +86 531 883 655 76; fax: +86 531 885 644 64; e-mail: yongjunliu_1@sdu.edu.cn.

Funding

This work was supported by the Natural Science Foundation of China (21173129, 21373125), the Research Award Foundation for Outstanding Young Scientists of Shandong Province (BS2013SW028), and the Taishan Scholars Climbing Program of Shandong Province.

Notes

The authors declare no competing financial interest.

ABBREVIATIONS:

Ub, ubiquitin; DUB, deubiquitinating enzyme; AMSH, associated molecule with the SH3 domain of STAM; JAMMs, JAB1/MPN/Mov34 metalloenzymes; K63-Ub_2, Lys63-linked diubiquitin; QM/MM, quantum mechanical/molecular mechanical method; RMSD, root-mean-square deviation; CPA, carboxypeptidase A; ACE, angiotensin-converting enzyme; IDE, insulin degrading enzyme; PES, potential energy surface

REFERENCES

(1) Ernst, A., Avvakumov, G., Tong, J., Fan, Y., Zhao, Y., Alberts, P., Persaud, A., Walker, J. R., Neculai, A. M., Neculai, D., Vorobyov, A., Garg, P., Beatty, L., Chan, P. K., Juang, Y. C., Landry, M. C., Yeh, C., Zeqiraj, E., Karamboulas, K., Allali-Hassani, A., Vedadi, M., Tyers, M., Moffat, J., Sicheri, F., Pelletier, L., Durocher, D., Raught, B., Rotin, D., Yang, J., Moran, M. F., Dhe-Paganon, S., and Sidhu, S. S. (2013) A strategy for modulation of enzymes in the ubiquitin system. *Science 339*, 590−595.

(2) Mattiroli, F., and Sixma, T. (2014) Lysine-targeting specificity in ubiquitin and ubiquitin-like modification pathways. *Nat. Struct. Mol. Biol. 21*, 308−316.

(3) Glickman, M. H., and Ciechanover, A. (2002) The ubiquitinproteasome proteolytic pathway: Destruction for the sake of construction. *Physiol. Rev. 82*, 373−428.

(4) Komander, D., and Rape, M. (2012) The ubiquitin code. Annu. *Annu. Rev. Biochem. 81*, 203−229.

(5) Varshavsky, A. (1997) The ubiquitin system. *Trends Biochem. Sci. 22*, 383−387.

(6) Shrestha, R. K., Ronau, J. A., Davies, C. W., Guenette, R. G., Strieter, E. R., Paul, L. N., and Das, C. (2014) Insights into the mechanism of deubiquitination by JAMM deubiquitinases from cocrystal structures of the enzyme with the substrate and product. *Biochemistry 53*, 3199−3217.

(7) Schulman, B., and Harper, J. W. (2009) Ubiquitin-like protein activation by E1 enzymes: The apex for downstream signaling pathways. *Nat. Rev. Mol. Cell Biol. 10*, 319−331.

(8) Hershko, A., and Ciechanover, A. (1998) The ubiquitin system. *Annu. Rev. Biochem. 67*, 425−479.

(9) Krutauz, D., Reis, N., Nakasone, M. A., Siman, P., Zhang, D., Kirkpatrick, D. S., Gygi, S. P., Brik, A., Fushman, D., and Glickman, M. H. (2014) Extended ubiquitin species are protein-based Dub inhibitors. *Nat. Chem. Biol. 10*, 664−670.

(10) Zhang, J., Zhang, X., Xie, F., Zhang, Z., van Dam, H., Zhang, L., and Zhou, F. (2014) The regulation of TGF-β/SMAD signaling by protein deubiquitination. *Protein Cell 5*, 503−517.

(11) Kulathu, Y., and Komander, D. (2012) Atypical ubiquitylation-the unexplored world of polyubiquitin beyond Lys48 and Lys63 linkages. *Nat. Rev. Mol. Cell Biol. 13*, 508−523.

(12) Meng, Q. S., Rao, L. Q., and Pan, Y. H. (2014) Enrichment and analysis of rice seedling ubiquitin-related proteins using four UBA domains (GST-qUBAs). *Plant Sci. 229*, 172−180.

DOI: 10.1021/acs.biochem.5b00527
Biochemistry 2015, 54, 5225−5234

(13) Dikic, I., Wakatsuki, S., and Walters, K. J. (2009) Ubiquitin-binding domains - from structures to functions. *Nat. Rev. Mol. Cell Biol. 10*, 659−671.
(14) Haglund, K., and Dikic, I. (2005) Ubiquitylation and cell signaling. *EMBO J. 24*, 3353−3359.
(15) Ikeda, F., and Dikic, I. (2008) Atypical ubiquitin chains: New molecular signals. 'Protein Modifications: Beyond the Usual Suspects' review series. *EMBO Rep. 9*, 536−542.
(16) Newton, K., Matsumoto, M. L., Wertz, I. E., Kirkpatrick, D. S., Lill, J. R., Tan, J., Dugger, D., Gordon, N., Sidhu, S. S., Fellouse, F. A., Komuves, L., French, D. M., Ferrando, R. E., Lam, C., Compaan, D., Yu, C., Bosanac, I., Hymowitz, S. G., Kelley, R. F., and Dixit, V. M. (2008) Ubiquitin chain editing revealed by polyubiquitin linkage-specific antibodies. *Cell 134*, 668−678.
(17) Guo, Z., Song, E., Ma, S., Wang, X., Gao, S., Shao, C., Hu, S., Jia, L., Tian, R., Xu, T., and Gao, Y. (2012) Proteomics strategy to identify substrates of LNX, a PDZ Domain-containing E3ubiquitin ligase. *J. Proteome Res. 11*, 4847−4862.
(18) Love, K., Catic, A., Schlieker, C., and Ploegh, H. (2007) Mechanisms, biology and inhibitors of deubiquitinating enzymes. *Nat. Chem. Biol. 3*, 697−705.
(19) D'Andrea, A., and Pellman, D. (1998) Deubiquitinating enzymes: A new class of biological regulators. *Crit. Rev. Biochem. Mol. Biol. 33*, 337−352.
(20) Komander, D. (2010) Mechanism, specificity and structure of the deubiquitinases. *Subcell. Biochem. 54*, 69−87.
(21) Nijman, S., Luna-Vargas, M., Velds, A., Brummelkamp, T., Dirac, A., Sixma, T., and Bernards, R. (2005) A genomic and functional inventory of deubiquitinating enzymes. *Cell 123*, 773−786.
(22) Komander, D., Clague, M. J., and Urbe, S. (2009) Breaking the chains: Structure and function of the deubiquitinases. *Nat. Rev. Mol. Cell Biol. 10*, 550−563.
(23) Wilkinson, K. D. (2009) DUBs at a glance. *J. Cell Sci. 122*, 2325−2329.
(24) Komada, M. (2008) Controlling receptor downregulation by ubiquitination and deubiquitination. *Curr. Drug Discovery Technol. 5*, 78−84.
(25) Clague, M. J., and Urbé, S. (2006) Endocytosis: the DUB version. *Trends Cell Biol. 16*, 551−559.
(26) Davies, C. W., Paul, L. N., and Das, C. (2013) Mechanism of recruitment and activation of the endosome-associated deubiquitinase AMSH. *Biochemistry 52*, 7818−7829.
(27) Zhou, J., Bi, D., Lin, Y., Chen, P., Wang, X., and Liang, S. (2012) Shotgun proteomics and network analysis of ubiquitin-related proteins from human breast carcinoma epithelial cells. *Mol. Cell. Biochem. 359*, 375−384.
(28) Emmerich, C. H., Ordureau, A., Strickson, S., Arthur, J. S., Pedrioli, P. G., Komander, D., and Cohen, P. (2013) Activation of the canonical IKK complex by K63/M1-linked hybrid ubiquitin chains. *Proc. Natl. Acad. Sci. U. S. A. 110*, 15247−15252.
(29) Meyer, H. J., and Rape, M. (2014) Enhanced protein degradation by branched ubiquitin chains. *Cell 157*, 910−921.
(30) Hospenthal, M. K., Mevissen, T. E. T., and Komander, D. (2015) Deubiquitinase-based analysis of ubiquitin chain architecture using Ubiquitin Chain Restriction (UbiCRest). *Nat. Protoc. 10*, 349−361.
(31) Sato, Y., Yoshikawa, A., Yamagata, A., Mimura, H., Yamashita, M., Ookata, K., Nureki, O., Iwai, K., Komada, M., and Fukai, S. (2008) Structural basis for specific cleavage of Lys 63-linked polyubiquitin chains. *Nature 455*, 358−362.
(32) Warshel, A., and Karplus, M. (1972) Calculation of ground and excited state potential surfaces of conjugated molecules. I. formulation and parametrization. *J. Am. Chem. Soc. 94*, 5612−5625.
(33) Warshel, A., and Levitt, M. (1976) Theoretical studies of enzymatic reactions: dielectric electrostatic and steric stabilization of the carbonium ion in the reaction of lysozyme. *J. Mol. Biol. 103*, 227−249.
(34) Xu, D. G., and Guo, H. (2009) Quantum mechanical/molecular mechanical and Density Functional Theory studies of a prototypical zinc peptidase (carboxypeptidase A) suggest a general acid-general base mechanism. *J. Am. Chem. Soc. 131*, 9780−9788.
(35) Zhang, C. C., Wu, S. S., and Xu, D. G. (2013) Catalytic mechanism of angiotensin-converting enzyme and effects of the chloride ion. *J. Phys. Chem. B 117*, 6635−6645.
(36) Zhang, T. T., Ozbil, M., Barman, A., Paul, T. J., Bora, R. P., and Prabhakar, R. (2015) Theoretical insights into the functioning of metallopeptidases and their synthetic analogues. *Acc. Chem. Res. 48*, 192−200.
(37) Pettersen, E. F., Goddard, T. D., Huang, C. C., Couch, G. S., Greenblatt, D. M., Meng, E. C., and Ferrin, T. E. (2004) UCSF Chimera-A visualization system for exploratory research and analysis. *J. Comput. Chem. 25*, 1605−1612.
(38) Li, H., Robertson, A. D., and Jensen, J. H. (2005) Very fast empirical pre-diction and rationalization of protein pKa values. *Proteins: Struct., Funct., Genet. 61*, 704−721.
(39) Bas, D. C., Rogers, D. M., and Jensen, J. H. (2008) Very fast prediction and rationalization of pKa values for protein-ligand complexes. *Proteins: Struct., Funct., Genet. 73*, 765−783.
(40) Olsson, M. H. M., Søndergaard, C. R., Rostkowski, M., and Jensen, J. H. (2011) PROPKA3: consistent treatment of internal and surface residues in empirical pKa predictions. *J. Chem. Theory Comput. 7*, 525−537.
(41) Søndergaard, C. R., Olsson, M. H. M., Rostkowski, M., and Jensen, J. H. (2011) Improved treatment of ligands and coupling effects in empirical calculation and rationalization of pKa values. *J. Chem. Theory Comput. 7*, 2284−2295.
(42) Brooks, B. R., Bruccoleri, R. E., Olafson, B. D., States, D. J., Swaminathan, S., and Karplus, M. (1983) CHARMM: a program for macromolecular energy, minimization, and dynamics calculations. *J. Comput. Chem. 4*, 187−217.
(43) Jorgensen, W. L., Chandrasekhar, J., Madura, J. D., Impey, R. W., and Klein, M. L. (1983) Comparison of simple potential functions for simulating liquid water. *J. Chem. Phys. 79*, 926−935.
(44) Chen, J. H., Im, W. P., and Brooks, C. L. (2006) Balancing solvation and intramolecular interactions: toward a consistent generalized born force field. *J. Am. Chem. Soc. 128*, 3728−3736.
(45) MacKerell, A. D., Jr., Bashford, D., Bellott, M., Dunbrack, R. L., Jr., Evanseck, J. D., Field, M. J., Fischer, S., Gao, J., Guo, H., Ha, S., Joseph-McCarthy, D., Kuchnir, L., Kuczera, K., Lau, F. T. K., Mattos, C., Michnick, S., Ngo, T., Nguyen, D. T., Prodhom, B., Reiher, W. E., III, Roux, B., Schlenkrich, M., Smith, J. C., Stote, R., Straub, J., Watanabe, M., Wiórkiewicz-Kuczera, J., Yin, D., and Karplus, M. (1998) All-atom empirical potential for molecular modeling and dynamics studies of proteins. *J. Phys. Chem. B 102*, 3586−3616.
(46) Brooks, C. L., Brünger, A., and Karplus, M. (1985) Active site dynamics in protein molecules: A stochastic boundary molecular-dynamics approach. *Biopolymers 24*, 843−865.
(47) de Vries, A. H., Sherwood, P., Collins, S. J., Rigby, A. M., Rigutto, M., and Kramer, G. J. (1999) Zeolite structure and reactivity by combined quantum-chemical-classical calculations. *J. Phys. Chem. B 103*, 6133−6141.
(48) Bakowies, D., and Thiel, W. (1996) Hybrid models for combined quantum mechanical and molecular mechanical approaches. *J. Phys. Chem. 100*, 10580−10594.
(49) Ahlrichs, R., Bar, M., Haser, M., Horn, H., and Kolmel, C. (1989) Electronic structure calculations on workstation computers: the program system turbomole. *Chem. Phys. Lett. 162*, 165−169.
(50) Lee, C., Yang, W., and Parr, R. G. (1988) Development of the Colle-Salvetti correlation-energy formula into a functional of the electron density. *Phys. Rev. B: Condens. Matter Mater. Phys. 37*, 785−789.
(51) Becke, A. D. (1993) Density-functional thermochemistry. III. The role of exact exchange. *J. Chem. Phys. 98*, 5648−5652.
(52) Smith, W., Forester, T. R. DL_POLY_2.0: a general-purpose parallel molecular dynamics simulation package. *J. Mol. Graphics 199614*, 136−141.10.1016/S0263-7855(96)00043-4
(53) Sherwood, P., de Vries, A. H., Guest, M. F., Schreckenbach, G., Catlow, C. R. A., French, S. A., Sokol, A. A., Bromley, S. T., Thiel, W.,

DOI: 10.1021/acs.biochem.5b00527
Biochemistry 2015, 54, 5225−5234

Turner, A. J., Billeter, S., Terstegen, F., Thiel, S., Kendrick, J., Rogers, S. C., Casci, J., Watson, M., King, F., Karlsen, E., Sjøvoll, M., Fahmi, A., Schäfer, A., and Lennartz, C. (2003) QUASI: a general purpose implementation of the QM/MM approach and its application to problems in catalysis. *J. Mol. Struct.: THEOCHEM 632*, 1−28.
(54) Billeter, S. R., Turner, A. J., and Thiel, W. (2000) Linear scaling geometry optimization and transition state search in hybrid delocalised internal coordinates. *Phys. Chem. Chem. Phys. 2*, 2177−2186.
(55) Nocedal, J. (1980) Updating quasi-Newton matrices with limited storage. *Math. Comput. 35*, 773−782.
(56) Liu, D. C., and Nocedal, J. (1989) On the limited memory method for large scale optimization. *Math. Prog. 45*, 503−528.
(57) Banerjee, A., Adams, N., Simons, J., and Shepard, R. (1985) Search for stationary-points on surface. *J. Phys. Chem. 89*, 52−57.
(58) Dolg, M., Wedig, U., Stoll, H., and Preuss, H. (1987) Energy-adjusted ab initio pseudopotentials for the first row transition elements. *J. Chem. Phys. 86*, 866−872.
(59) Grimme, S., Antony, J., Ehrlich, S., and Krieg, H. (2010) A consistent and accurate ab initio parametrization of density functional dispersion correction (DFT-D) for the 94 elements H-Pu. *J. Chem. Phys. 132*, 154104−154123.
(60) Holden, H. M., Tronrud, D. E., Monzingo, A. F., Weaver, L. H., and Matthews, B. W. (1987) Slow- and fast-binding inhibitors of thermolysin display different modes of binding: crystallographic analysis of extended phosphonamidate transition-state analogues. *Biochemistry 26*, 8542−8553.

DOI: 10.1021/acs.biochem.5b00527
Biochemistry 2015, 54, 5225−5234